1

A Single-Step Multiclass SVM based on Quantum Annealing for Remote Sensing Data Classification

Amer Delilbasic, Student Member, IEEE, Bertrand Le Saux, Senior Member, IEEE, Morris Riedel, Member, IEEE, Kristel Michielsen, and Gabriele Cavallaro, Senior Member, IEEE

Abstract—In recent years, the development of quantum annealers has enabled experimental demonstrations and has increased research interest in applications of quantum annealing, such as in quantum machine learning and in particular for the popular quantum Support Vector Machine (SVM). Several versions of the quantum SVM have been proposed, and quantum annealing has been shown to be effective in them. Extensions to multiclass problems have also been made, which consist of an ensemble of multiple binary classifiers. This work proposes a novel quantum SVM formulation for direct multiclass classification based on quantum annealing, called Quantum Multiclass SVM (QMSVM). The multiclass classification problem is formulated as a single quadratic unconstrained binary optimization problem solved with quantum annealing. The main objective of this work is to evaluate the feasibility, accuracy, and time performance of this approach. Experiments have been performed on the D-Wave Advantage quantum annealer for a classification problem on remote sensing data. Results indicate that, despite the memory demands of the quantum annealer, OMSVM can achieve an accuracy that is comparable to standard SVM methods, such as the one-versus-one (OVO), depending on the dataset (compared to OVO: 0.8663 vs 0.8598 on Toulouse, 0.8123 vs 0.8521 on Potsdam). More importantly, it scales much more efficiently with the number of training examples, resulting in nearly constant time (compared to OVO: 85.72s vs 248.02s on Toulouse, 58.89s vs 580.17s on Potsdam). This work shows an approach for bringing together classical and quantum computation, solving practical problems in remote sensing with current hardware.

Index Terms—Support Vector Machine (SVM), Quantum Computing (QC), Quantum Annealing (QA), classification, Remote Sensing (RS)

I. INTRODUCTION

N the context of Earth Observation (EO) [1], there is a growing availability of data acquired by heterogeneous Remote Sensing (RS) sources. Many applications are currently benefitting from RS data, e.g., agriculture, green energy development and urban monitoring. The devices and software for

Amer Delilbasic is with the Jülich Supercomputing Centre, Wilhelm-Johnen Straße, 52428 Jülich, Germany, with the University of Iceland, 107 Reykjavik, Iceland, and with ESA/ESRIN Φ -lab, IT-00044 Frascati, Italy (e-mail: a.delilbasic@fz-juelich.de).

Bertrand Le Saux is with ESA/ESRIN Φ -lab, IT-00044 Frascati, Italy (e-mail: bertrand.le.saux@esa.int).

Morris Riedel and Gabriele Cavallaro are with the University of Iceland, 107 Reykjavik, Iceland, with the Jülich Supercomputing Centre, Wilhelm-Johnen Straße 52428 Jülich, Germany and with the AIDAS, 52425 Jülich, Germany (e-mail: morris@hi.is, g.cavallaro@fz-juelich.de).

Kristel Michielsen is with the Jülich Supercomputing Centre, Wilhelm-Johnen Straße 52428 Jülich, Germany, with the RWTH Aachen University, D-52056 Aachen, Germany, and with the AIDAS, 52425 Jülich, Germany (e-mail: k.michielsen@fz-juelich.de).

TABLE I ABBREVIATIONS USED IN THE ARTICLE.

AQC	adiabatic quantum computation
BDSD	band-dependent spatial-detail
CS	Crammer-Singer
DAG	directed acyclic graph
DSM	digital surface model
EO	Earth observation
ML	machine learning
OVA	one-versus-all
OVO	one-versus-one
QA	quantum annealing
QC	quantum computing
QML	quantum machine learning
QMSVM	quantum multiclass support vector machine
QSVM	quantum support vector machine
QUBO	quadratic unconstrained binary optimization
RS	remote sensing
SVM	support vector machine

data processing have to match this trend in order to extract information from the collected data in a timely manner.

Quantum Computing (QC) [2], a computational paradigm based on the postulates and laws of quantum mechanics, has proved the potential to reach an exponential algorithmic speedup with respect to classical computation under certain assumptions [3], [4]. Among the quantum computational models defined in the literature, two broadly employed models can be identified. The quantum circuit model [5], similarly to the classical circuit model, is based on circuits, gates and measurements applied to qubits (quantum bits). Adiabatic Quantum Computation (AQC) [6], [7] aims at solving optimization problems by exploiting the time evolution of a quantum system satisfying the requirements of the adiabatic theorem [8]. Despite their differences, the two models have been proven to be computationally equivalent [9]. The focus of this work is Quantum Annealing (QA) [10], [11], a heuristic search approach based on AQC, since commercially ready quantum annealers are available for analyzing the disruptive potential of QC.

Quantum Machine Learning (QML) [12], [13] is a research area working on QC algorithms applied to Machine Learning (ML) tasks, with the purpose of obtaining a computational speedup or a prediction accuracy increase. QML methods based on QA have proven to outperform classical ML in selected applications with limited training examples, for example in computational biology [14]. Recent studies have analyzed how QML can be integrated into EO tasks. In [15], [16], [17], [18], circuit-based quantum neural networks have been trained for multispectral image classification. The

work of Otgonbaatar and Datcu has covered different aspects of circuit-based QML for EO, e.g., natural data embedding [19], parameterized quantum gates [20] and transfer learning [21]. Circuit-based quantum kernels have been applied to binary [22], [23], [24] and multiclass [25] RS image classification. QA has also found a place in EO for solving specific optimization problems. In Synthetic Aperture Radar (SAR) imaging, problems related to system design [26] and phase ambiguity [27] have been addressed. In the context of QML, a feature selection method for hyperspectral images has been proposed [28], and a QA-based Quantum Support Vector Machine (QSVM) method has been successfully used for binary classification of multispectral images [29] [30].

The Support Vector Machine (SVM) is an efficient and theoretically-grounded algorithmic approach in statistical learning theory. Different versions and formulations of the SVM can be found in the literature for a variety of tasks and applications, e.g., pattern recognition, computer vision, image analysis and business intelligence [31]. SVM has also been proven to be effective in EO pixel-wise image classification [32].

Defining a SVM framework for multiclass classification is a non-trivial task. Two different approaches can be followed [33]. The multiple-step (or indirect) approach reframes the problem by defining an ensemble of multiple binary SVM classifiers and multiple classification outputs. The most common methods are the one-versus-one (OVO), one-versus-all (OVA) and the Directed Acyclic Graph (DAG) SVM. In the OVO method, each pair of classes defines a SVM classifier. The outcomes of each classifier are usually combined with a "max wins" strategy which determines the final prediction. Similarly, in the OVA method, a classifier for each class vs. the remaining classes is defined, and the class with highest score is assigned. The QSVM algorithms for multiclass classification available in the literature, e.g., [34], [35], [36], follow the multi-step approach. They are defined as ensembles of binary QSVM classifiers, which can be full quantum [37], [38], quantumkernel-based [39] and QA-based [40] formulations.

The *single-step* (or *direct*) *approach* for multiclass classification defines a single optimization step on the whole training set, which finds boundaries between all classes in one pass. The Crammer-Singer (CS) SVM, proposed in [41], is an example of single-step approach. It showed a comparable to better performance on benchmark datasets with respect to OVO, OVA, and the Weston-Watkins [42] multiclass SVM [43]. However, a limitation of this method is the complexity of the training phase, due to the high number of optimization variables, which makes this approach impractical. In the same work, simplified formulations are proposed, which reduce the problem size and enable better performances, although at the cost of optimality.

The main objective of this work is to propose a novel approach, specifically Quantum Multiclass SVM (QMSVM), by reframing the original formulation of the CS SVM, thus enabling the optimization step to be performed using a QA algorithm. This work studies the computational capability offered by the available quantum annealers and assesses the feasibility of a QA-based single-step SVM approach. Experi-

ments are performed on a real quantum annealer, i.e., D-Wave Advantage [44], [45], in order to validate the algorithm on current hardware. As quantum annealers are a rapidly evolving technology, it is important to analyze their current status and their potential, understanding how they can be used to solve real problems in RS. For this purpose, it is reasonable to consider the CS SVM implementation in our work, as it is a computationally intensive task that would benefit from an enhanced performance. The performance is evaluated both in terms of accuracy and execution time, both relevant aspects in practice. The code repository of the algorithm is made available for reproducibility¹.

The paper is structured as follows. In Sect. II, the theoretical background related to quantum annealing is summarized. In Sect. III, the mathematical formulation of QMSVM is presented. In Sect. IV, the algorithm validation setup is described and the results are shown. In Sect. V, the main findings are discussed. In Sect. VI, conclusions related to the presented work are drawn.

II. BACKGROUND

A. Quantum Annealing and QUBO

To understand the underlying working principles of D-Wave quantum annealers, a brief introduction is needed. In AQC [6], [7], the forces acting in a quantum system are described by a time-varying Hamiltonian $\mathcal{H}(t)$. The time evolution of the state of a quantum system $|\varphi(t)\rangle$ is described by the Schrödinger's Equation:

$$i\hbar \frac{\partial |\varphi(t)\rangle}{\partial t} = \mathcal{H}(t) |\varphi(t)\rangle$$
 (1)

where i is the imaginary unit and \hbar is the reduced Planck constant. During the adiabatic evolution, the Hamiltonian gradually transitions from the initial Hamiltonian \mathcal{H}_I to the final Hamiltonian \mathcal{H}_F :

$$\mathcal{H}(t) = s(t)\mathcal{H}_I + (1 - s(t))\mathcal{H}_F \tag{2}$$

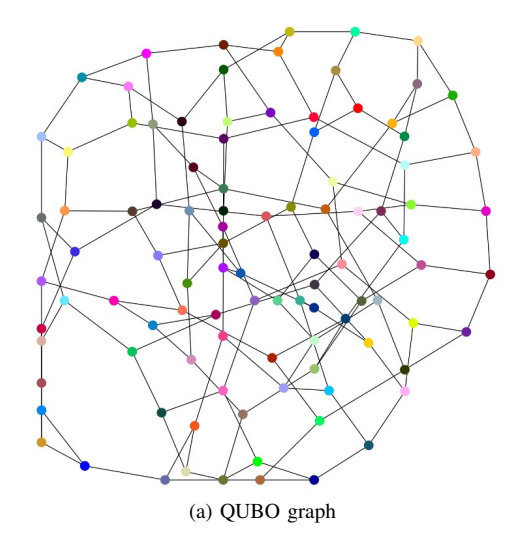
where s(t) is a function modeling the transition, such that s(0) = 1 and $s(t_f) = 0$ after a certain elapsed time t_f . Given the assumptions of the adiabatic theorem [8], during the time evolution, the quantum system remains at ground state, i.e., the state with lowest energy associated with the Hamiltonian. The idea in AQC is to encode the desired result as the ground state of the final Hamiltonian \mathcal{H}_F .

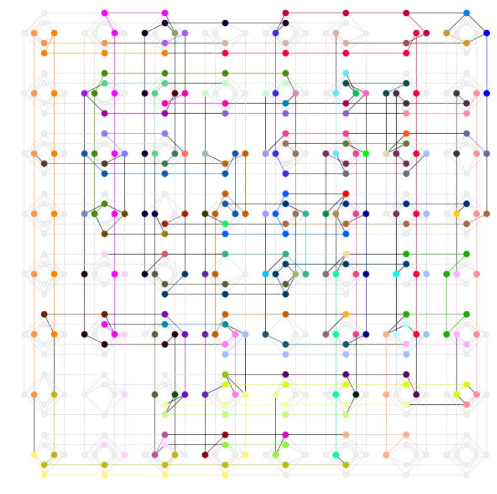
QA falls into the category of AQC algorithms. More precisely, it is a heuristic approach for solving combinatorial optimization problems. In this case, the Hamiltonian of the system is defined as:

$$\mathcal{H}(t) = \mathcal{H}_F + \Gamma(t)\mathcal{H}_D \tag{3}$$

where \mathcal{H}_F is the final Hamiltonian, $\Gamma(t)$ is the transverse field coefficient as a function of time t, and \mathcal{H}_D is the transverse field Hamiltonian (also called disorder Hamiltonian). \mathcal{H}_F encodes the objective function and its ground state is the solution of the optimization problem. $\Gamma(t)$ is a decreasing function, equal to 0 for $t=t_f$. It controls the contribution

¹ https://gitlab.jsc.fz-juelich.de/sdlrs/qmsvm





(b) Embedding of the QUBO graph on a Pegasus architecture

Fig. 1. Graphical representation of the minor embedding step. In the graph shown in (a), each node represents a binary variable, and each edge represents a logical connection between two variables of the QUBO problem. In (b), each color represents the corresponding variable embedded into a qubit chain. Source: [6]

of \mathcal{H}_D , which enables traversability of the solution space, making the optimization process escape local minima. As for this aspect, QA presents a similarity with simulated annealing [46], where the temperature parameter T resembles the role of $\Gamma(t)$. In this framework, the assumptions of the adiabatic theorem are relaxed, i.e., there is no requirement for the quantum system to be closed and to operate in the ground state. The implementation of QA provided by D-Wave quantum annealers enables the solution of a specific type of optimization problems, called Quadratic Unconstrained Binary Optimization (QUBO) problems. A QUBO problem is defined as:

minimize
$$\sum_{i < j} a_i Q_{ij} a_j \tag{4}$$

where $a_i \in \{0,1\}$ are the binary variables of the problem and Q an upper-triangular matrix called QUBO matrix.

B. Minor Embedding

The hardware architecture of D-Wave quantum annealers poses a limitation on the OUBO problems that can be solved. The most relevant specifications are the number of qubits, the number of couplers (i.e., the physical connections between pairs of qubits) and the qubit connectivity (i.e., the average number of couplers connected to a qubit). D-Wave Advantage is based on the Pegasus architecture and has approximately 5000 qubits, 35000 couplers, and a qubit connectivity of 15 [45]. When the QUBO problem is submitted to a quantum annealer, a step called *minor embedding* [47] is performed, in which each binary variable of the problem a_i is embedded into a qubit chain. The main requirement is maintaining the logical structure of the problem, described by Q. Each element of the QUBO matrix Q_{ij} represents a logical relation between the variables a_i and a_j . The coefficients Q_{ij} are mapped to the strength of the couplers connecting the qubit chains assigned to

the variables a_i and a_j . The existence of such an embedding is a requirement for a problem to be solved by the annealer, i.e., constraints on the dimension and the structure of the QUBO problem need to be satisfied. In Fig. 1, the embedding of a QUBO problem in graph form is shown.

III. QUANTUM MULTICLASS SVM FORMULATION

In this section, a novel algorithm called QMSVM is described. It is based on a reformulation of the Crammer-Singer (CS) SVM [41] as a QUBO problem. The followed steps are adapted from the QSVM proposed in [40], with the addition of a solution combination method. As a starting point, the CS SVM formulation is described in the following.

A. Crammer-Singer Multiclass SVM

In a supervised multiclass classification problem, let N be the number of training examples, C the number of classes, $X^{tr} = \{\mathbf{x}_n\}$ the feature vectors of dimension $F, Y^{tr} = \{y_n\}$ the labels. The training consists in the solution of the following quadratic program:

minimize
$$F(T) = \frac{1}{2} \sum_{n_1, n_2 = 0}^{N-1} K(\mathbf{x}_{n_1}, \mathbf{x}_{n_2}) \sum_{c=0}^{C-1} \tau_{n_1 c} \tau_{n_2 c}$$

$$-\beta \sum_{n=0}^{N-1} \sum_{c=0}^{C-1} \delta_{cy_n} \tau_{nc}$$
(5)

subject to
$$\sum_{c=0}^{C-1} \tau_{nc} = 0 \quad \forall n, \quad \tau_{nc} \leq 0 \quad \forall n, \forall c \neq y_n.$$

where $T=[\tau_{nc}]$ is the matrix of the NC problem variables, with $n=0,...,N-1,\,c=0,...,C-1$ and $\tau_{nc}\in[-1,1],\,\delta_{ij}$ is the Kronecker delta and β a regularization parameter.

D-Wave Advantage is unable to directly solve Eq. (5)-(6). Therefore, a reformulation of Eq. (5)-(6) as a QUBO

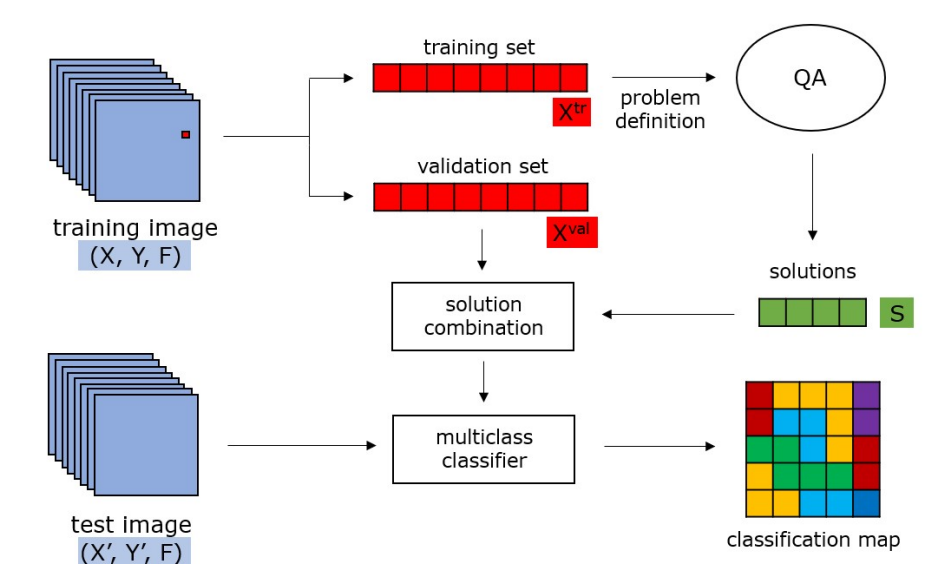


Fig. 2. Flowchart of the QMSVM algorithm. A training set X^{tr} is given as input to the QA step, which obtains a set of S solutions to the training problem. The solutions are then combined with a weighted average based on the accuracy performance on a validation set X^{val} of the classifiers obtained by the single solutions. The final classifier is then used to generate classification maps of test images.

problem is necessary. The followed steps are: choosing a binary encoding (Sect. III-B), defining the penalty terms (Sect. III-C), deriving the QUBO matrix including the results of the previous steps in the cost function (Sect. III-D), and defining a solution combination method (Sect. III-E).

B. Binary Encoding

The first step consists in defining the binary variables a_i of the QUBO problem. In the CS formulation, the problem variables τ_{nc} are real numbers. The idea is to discretize the solution space using uniform sampling and represent each value as a set of B binary variables. First, the following intermediate variable is defined:

$$\sigma_{nc} = \sum_{b=0}^{B-1} 2^b a_{nCB+cB+b}.$$
 (7)

 σ_{nc} is an integer value in $[0,2^B-1]$ represented by the binary encoding $\{a_{nCB+cB+b}\}, b=0,\ldots,B-1$. Then, the problem variables τ_{nc} can be defined from σ_{nc} as:

$$\tau_{nc} = -1 + \frac{2}{2^B - 1}\sigma_{nc} = -1 + \frac{2}{2^B - 1}\sum_{b=0}^{B-1} 2^b a_{nCB+cB+b}.$$
(8)

With this definition, it can be proven that each value of τ_{nc} lies in [-1,1] and the interval is uniformly sampled.

Fig. 3 shows the sampling of Eq. (8) for B=2, i.e., in the case each sample of τ_{nc} is represented by 2 binary variables, indicated above each sample. Since the total number of problem variables is NC (each variable is associated with an example and a class), the whole optimization space can be represented by a set of NCB binary variables $\{a_0, a_1, ..., a_{NCB-1}\}$.

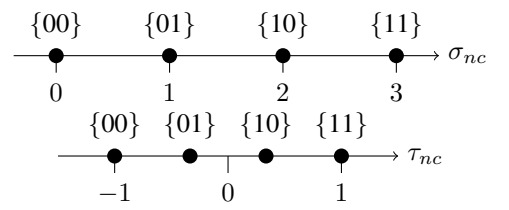


Fig. 3. Representation of the chosen variable sampling and encoding for B=2

C. Penalty Terms

Another requirement is to include the constraints of Eq. (6), as no constraints can be directly enforced in a QUBO problem. A possibility is to add the constraints to the QUBO matrix as weighted positive penalty terms. For the first constraint, the penalty term needs to increase in the case the difference between the value of the sum and 0 increases. In addition, a penalty term needs to be associated with each training example and with the same weight. Since a quadratic polynomial term is required, the following penalty term is chosen:

$$P_n^1 = \left(\sum_{c=0}^{C-1} \tau_{n,c}\right)^2 \tag{9}$$

For the second constraint, which is an inequality, it is sufficient to directly consider τ_{nc} as the penalty term associated with each training sample and each class. A coefficient $(1-\delta_{cy_n})$ is attached to account for the case $c=y_n$, in which the penalty is zero:

$$P_{nc}^2 = (1 - \delta_{cy_n})\tau_{n,c} \tag{10}$$

The final penalty term can be written as:

$$P = \sum_{n=0}^{N-1} P_n^1 + \sum_{n=0}^{N-1} \sum_{c=0}^{C-1} P_{nc}^2$$

$$= \sum_{n=0}^{N-1} \left(\sum_{c=0}^{C-1} \tau_{n,c}\right)^2 + \sum_{n=0}^{N-1} \left(\sum_{c=0}^{C-1} (1 - \delta_{cy_n}) \tau_{n,c}\right)$$
(11)

Note that P_n^1 and P_{nc}^2 are included with the same weight. The following reasons behind this choice can be listed:

- Considering two different weights would increase the number of hyperparameters of the optimization problem and the already high complexity of the tuning phase;
- The two constraints have to be both equally satisfied;
- The two penalty terms have approximately the same order of magnitude, as $\tau_{nc} \in [-1,1]$, so there is no imbalance in values.

D. QUBO Matrix

The QUBO problem can be now written by adding to Eq. (5) the penalty term in Eq. (11) multiplied by a weight μ and substituting $\tau_{i,j}$ with the encoding in Eq. (8). The energy function E can be written in the following form²:

$$E = F + \mu P = \sum_{n_1 n_2 c_1 c_2 b_1 b_2} a_{n_1 CB + c_1 B + b_1}$$

$$\tilde{Q}_{n_1 CB + c_1 B + b_1, n_2 CB + c_2 B + b_2} a_{n_2 CB + c_2 B + b_2}.$$
(12)

 \widetilde{Q} is a symmetric matrix of size $NCB \times NCB$. It can be analytically derived by neglecting the terms not depending on the binary variables and is equal to:

$$\widetilde{Q}_{n_{1}CB+c_{1}B+b_{1},n_{2}CB+c_{2}B+b_{2}} =
= \delta_{n_{1}n_{2}}\delta_{c_{1}c_{2}}\delta_{b_{1}b_{2}}\frac{2^{b_{1}+1}}{2^{B}-1}\left(-\sum_{i}K(\mathbf{x}_{n_{1}},\mathbf{x}_{i})\right)
- \delta_{c_{1}y_{n_{1}}}(\beta+\mu) - 2C\mu + \mu\right)
+ \delta_{c_{1}c_{2}}\frac{2^{b_{1}+b_{2}+1}}{(2^{B}-1)^{2}}K(\mathbf{x}_{n_{1}},\mathbf{x}_{n_{2}}) + \delta_{n_{1}n_{2}}\frac{2^{b_{1}+b_{2}+2}\mu}{(2^{B}-1)^{2}}$$
(13)

The upper-triangular QUBO matrix Q can be computed from \widetilde{Q} as:

$$Q_{ij} = \begin{cases} \widetilde{Q}_{ij} & \text{for } i = j\\ \widetilde{Q}_{ij} + \widetilde{Q}_{ji} & \text{for } i < j\\ 0 & \text{otherwise} \end{cases}$$
 (14)

E. Solution Combination

Once the QUBO matrix is defined, the problem can submitted to the quantum annealer, assuming the existence of an embedding. As the annealing process is performed multiple times, depending on the value of num_reads , the obtained output is a set of num_reads solutions. The best S solutions are selected, i.e., $T_i = [\tau_{nc}]_i$, $i = 0, \ldots, S-1$, ranked by the

value of the energy function $E(T_i)$. During the experiments, it has been noticed that there is no perfect correlation between solutions with lower energy and better classification accuracy of the obtained classifier. Note also that the solution space investigated by the quantum annealing algorithm is discrete, due to the variable sampling, so the obtained individual solutions are likely to be sub-optimal. For these reasons, a solution combination is performed in order to obtain an optimal final solution. A weighted average is performed, where the weights w_s for each solution s are set according to the prediction accuracy of the obtained classifiers on a validation set $\{X^{val}, Y^{val}\}$. In particular, the solutions above a certain threshold accuracy are selected, and their weight is computed applying the softmax function to multiplier \cdot accuracy_s, where multiplier is a real value and accuracy, is the accuracy of the classifier defined by the s-th solution on the whole training set. The rest of the weights are set to 0. The combined solution is computed as:

$$\bar{T} = \frac{1}{S} \sum_{s=0}^{S-1} w_s T_s. \tag{15}$$

The resulting variables $\bar{\tau}_{nc}$ are then used to classify new examples:

$$H(\mathbf{x}) = \arg\max_{c} \left\{ \sum_{n=0}^{N-1} \bar{\tau}_{nc} K(\mathbf{x}, \mathbf{x}_{n}) \right\}$$
(16)

Alg. 1 summarizes the implemented computational steps required for the training.

Algorithm 1 Quantum Multiclass SVM (QMSVM)

Input: $X^{tr}, Y^{tr}, X^{val}, Y^{val}, C, B, \beta, \mu, \gamma, S$, multiplier Output: \bar{T}

QUBO matrix initialization, eq. (13)-(14)

1: $Q \leftarrow \text{QUBO_MATRIX}(X^{tr}, Y^{tr}, C, B, \beta, \mu, \gamma)$

Run annealing step and sample num_reads solutions

2: $T \leftarrow \text{QUANTUM_ANNEALING}(Q)$

Evaluate classifier on validation set, eq. (16)

3: **for** s = 1 to S **do**

4: $\hat{Y}^{val}[s] \leftarrow H(X^{val}, Y^{val}, T)$

5: $accuracy[s] \leftarrow ACCURACY(\hat{Y}^{val}[s], Y^{val})$

6: end for

Weights calculation

7: threshold ← THRESHOLD(accuracy)

8: for s=1 to S do

9: **if** accuracy[s] < threshold **then**

 $accuracy[s] \leftarrow 0$

11: end if

12: end for

10:

13: $W \leftarrow \text{SOFTMAX}(\text{multiplier} \cdot \text{accuracy})$ Solution combination, eq. (15)

14: $\bar{T} \leftarrow \text{COMBINE}(T, W)$

15: **return** \overline{T}

IV. ALGORITHM VALIDATION

A. Experimental Setup

The QMSVM algorithm has been validated on a semantic segmentation problem applied to multispectral RS images.

²In this formulation, a simplified notation for the sums is used, as the range of the indices is unaltered and redundant.

TABLE II
DATASETS USED IN THE EXPERIMENTS.

Dataset	Dimension	Resolution	Features	Classes	Training Set	Test Set
SemCity Toulouse [48]	16 tiles, 3504×3452	50 cm	8 bands	$C \le 7$	N samples, tile 4	800×800 area, tile 8
ISPRS Potsdam [49]	38 tiles, 6000×6000	5 cm	4 bands + DSM	$C \le 5$	N samples, tile 6_9	1000×1000 area, tile 6_10

TABLE III PARAMETERS SETUP.

Variable Name	Value	Description			
C	3	Number of classes considered in the multiclass classification problem			
B	2	Number of binary variables representing each problem variable $ au_{nc}$			
β	0.1	Model related regularization parameter, introduced in Eq. (5)			
μ	1	Weight of the penalty term P added to the energy function defined in Eq. (12)			
γ	0.5	Gaussian kernel parameter, regulating its radius			
N	[50, 20000]	Total number of training examples used in the training (multiple values analyzed)			
M	60	Number of selected training examples, used to define the QUBO matrix Q submitted to the QA			
num_reads	1000	Number of times the annealing schedule is performed and how many solutions are sampled for each run			
S	100	Number of solutions selected among the total number num_reads, used for the solution combination			
multiplier	10	Regulates the balance between higher and lower accuracy values over the combined solutions			
max_min_ratio	5	Ratio between the maximum and minimum non-zero absolute value of the QUBO matrix Q			
chain_strength	1	Relative coupling strength between qubits that form a chain and qubits in different chains			
annealing_time	100	Time (in µs) at which the measurement is performed after starting the annealing schedule			

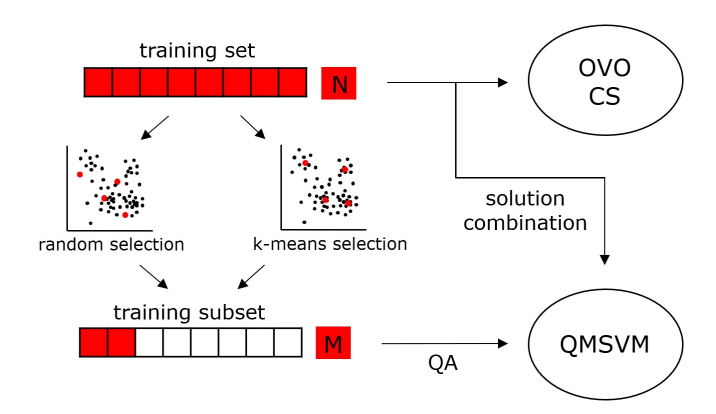


Fig. 4. Training setup. The OVO and CS methods have been trained on a training set of N examples. For QMSVM, a subset of M examples is selected and used by the annealing algorithm, while the solution combination is performed based on the accuracy obtained on the whole training set.

Two different datasets are considered, i.e., SemCity Toulouse [48] (hereafter "Toulouse") and ISPRS Potsdam [49] (hereafter "Potsdam"). Tab. II describes the selected datasets. While both represent urban areas, the two datasets differ in the features and the ground resolution. Toulouse is based on 8-band Worldview-2 data. We chose the 50 cm multispectral images obtained through pansharpening of the 2 m multispectral data with 50 cm panchromatic images using the Band-Dependent Spatial-Detail (BDSD) algorithm. Potsdam is based on aerial data collection and, on top of 4 spectral bands, a Digital Surface Model (DSM) is provided, which is used as a feature. The complete ground truths are obtained by expert annotators. For each dataset, 5 training sets of N examples are randomly initialized, from the training tiles indicated in Tab. II..

The experiments have been performed on a real quantum device, JUPSI [50], a D-Wave Advantage quantum annealer located at Forschungszentrum Jülich. To access the machine, the $Advantage_system5.4$ cloud solver has been used. Given the memory and connectivity limitation of the machine, the training set $\{X^{tr}, Y^{tr}\}$ defined in Sect. III-A is initialized as a subset of M examples from the total number of training examples N. The training subset is computed through an example selection step. Two selection methods have been tested:

- Random selection: M random examples are selected from the whole training set. It is a fast and straightforward method, enforcing no selection criterion.
- K-means selection: k-means clustering [51] is applied to each of the C classes, with k = M/C, and the obtained M centroids are used as selected examples. It is inspired by undersampling techniques in imbalanced classification [52]. In principle, the method is designed to select meaningful examples, covering the whole feature domain.

The whole training set is then used as the validation set $\{X^{val}, Y^{val}\}$ for the solution combination, introduced in Sect. III-E³. The *threshold* accuracy, which determines which solutions are discarded in the combination, has been computed as:

threshold = $0.2 \cdot \min(\text{accuracy}) + 0.8 \cdot \max(\text{accuracy})$. (17)

The results are compared with three standard implementations of the multiclass SVM, i.e., the OVO and OVA imple-

³Note that the training sets are named differently here. In the formulation, the general terms "training set" and "validation set" are used, coherently with ML literature. Here, the terms "training subset" and "training set" are used respectively, coherently with our training setup, which is far from being universal.

TABLE IV
RESULTS OF ACCURACY, F1 SCORE AND EXECUTION TIME FOR OVO AND QMSVM.

Solver	N	M	Accuracy	F1	t (s)				
Toulouse - best accuracy, maximum N									
OVO	20000	-	0.8598	0.8612	248.02				
OVA	20000	-	0.8606	0.8617	595.50				
CS	20000	-	0.8213	0.8279	1007.19				
QMSVM (random)	20000	60	0.8663	0.8721	245.39				
QMSVM (k-means)	20000	60	0.8133	0.8178	85.72				
Potsdam - best accuracy, maximum N									
OVO	15000	-	0.8521	0.8530	580.17				
OVA	15000	-	0.8514	0.8523	1317.35				
CS	15000	-	0.8226	0.8362	2708.62				
QMSVM (random)	15000	60	0.7695	0.7840	84.20				
QMSVM (k-means)	15000	60	0.8123	0.8143	58.89				

mentation in Scikit-learn [53] and a CS SVM implementation in C++ [54]. A Gaussian kernel with parameter γ is chosen. The training setup is depicted in Fig. 4.

B. Parameters

In Tab. III the parameters of the problem are described. The parameters β , μ and γ are set through a simple grid search optimization, training the model on a smaller training subset of 20 examples and validating it on the whole training set. Different values of N are chosen in order to analyze the performance of the method by varying the number of available examples. The highest tested value is N=20000 for Toulouse and N=15000 for Potsdam. The parameters B, M and max min ratio are related to the main limitation of the QA, i.e., the number of qubits and couplers. As previously discussed, finding an embedding on the given qubit architecture is required for solving the QUBO problem. This is achieved in case Q is sufficiently small, sufficiently sparse, or both. Using only the selected training subset, the dimension of Q is MCB. Thus, M is limited, which is the reason the QA is unable to use an arbitrarily large training set and example selection is performed in the first place. To maximize the number of examples fitting in the QA, the remaining parameters are kept low, i.e., C=3 and B=2. Considering a higher number of classes, i.e., C > 3, would require using a lower number of examples M, which degrades the overall performance. Regarding sparsity, a straightforward operation is performed, i.e., pruning the values of Q below the threshold defined by max min ratio, chosen empirically. This simplification is acceptable, as relatively low values would be mapped to relatively low strengths in the QA, which mildly affect the annealing process. The parameters num_reads, chain_strength and annealing_time are related to the annealer setup. Their values are chosen empirically, finding a trade-off between total run time and quality of the solutions on the small validation set, testing a range of values that have been considered valid in previous work, e.g., in [55]. The remaining parameters are set arbitrarily. Tab. III summarizes the chosen parameter values.

C. Results

In the test phase, the methods are evaluated on a 3-class classification problem on a selected area taken from the dataset. For Toulouse, a 800×800 test area from tile 8 has been selected and the classes "building", "pervious surface", "water" have been considered. For Potsdam, a 1000×1000 test area from tile 6_10 has been selected and the classes "building", "low vegetation", "tree" have been considered.

The method is evaluated according to both test accuracy and execution time. For OVO, OVA and CS, training and inference are considered. For QMSVM, the time measurement includes preprocessing (example selection), training (annealing), post-processing (solution combination) and inference time. Fig. 5-6 shows the ground truth of the selected area and the ground maps obtained by OVO, CS and QMSVM. In Fig. 7-10 the performance of the analyzed methods on the Toulouse and Potsdam dataset is shown in terms of both test accuracy and execution time, and for both example selection methods, i.e., random and k-means selection. Tab. IV summarizes the best obtained results in terms of test accuracy, along with the respective F_1 score. Accuracy and F_1 score are computed as:

accuracy =
$$\frac{\text{correct predictions}}{\text{no. of predictions}}$$
, $F_1 = \text{average}_c(F_{1c})$.

 F_{1c} is the F_1 score computed for each class c with respect to the remaining classes:

$$F_{1c} = \frac{\text{TP}_c}{\text{TP}_c + \frac{1}{2}(\text{FN}_c + \text{FP}_c)},$$
 (19)

where TP (true positive), FN (false negative) and FP (false positive) predictions are referred to the class c. For each method, the average results on the 5 training sets are plotted and the space between the best and the worst obtained results is highlighted. For CS, experiments on only one training set have been performed, due to the slow training.

V. DISCUSSION

A. QMSVM on D-Wave Advantage

Running the proposed algorithm on the D-Wave Advantage quantum annealer requires particular attention to its functioning. First of all, a QUBO formulation needs to be derived from the original problem, which is not always possible. The analytical derivation we provided successfully reframed the problem, although with some inevitable changes and arbitrary choices, e.g., on the optimization variable domain and the constraint satisfaction. Then, as previously mentioned, the main limitation of quantum annealers is in the maximum problem size that can be submitted. We tackle this limitation by using only a small subset of the training set and then refining the obtained solutions using the whole training set. Understanding how many examples we should consider and how sparse the QUBO matrix should be requires some experience given by trial and error. The parameters provided can be used as a reference for future work.

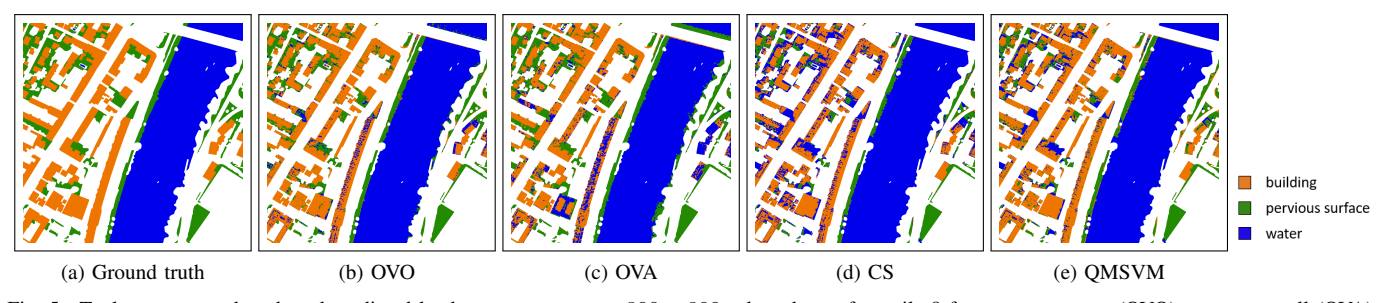


Fig. 5. Toulouse - ground truth and predicted land cover maps on an 800×800 selected area from tile 8 for one-versus-one (OVO), one-versus-all (OVA), Crammer-Singer (CS) and Quantum Multiclass SVM (QMSVM) using N=20000 training examples. The considered classes are "building" (orange), "pervious surface" (green) and "water" (blue).

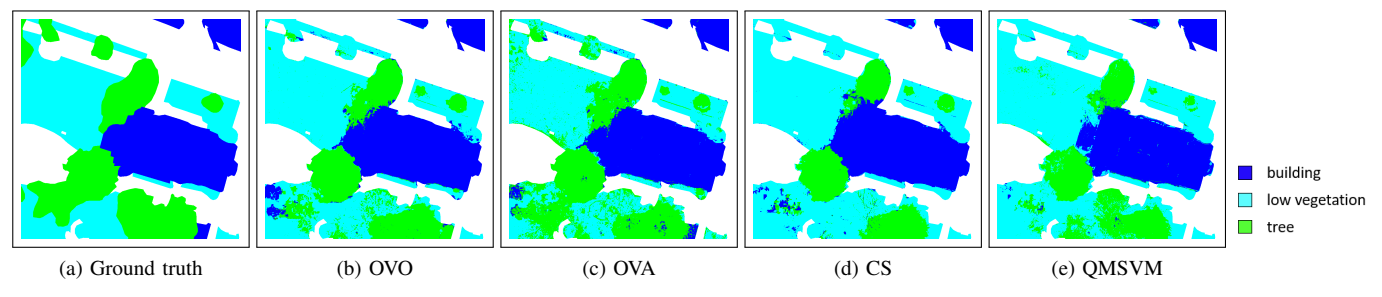


Fig. 6. Potsdam - ground truth and predicted land cover maps on a 1000×1000 selected area from tile 6_10 for one-versus-one (OVO), one-versus-all (OVA), Crammer-Singer (CS) and Quantum Multiclass SVM (QMSVM) using N=15000 training examples. The considered classes are "building" (blue), "low vegetation" (light blue) and "tree" (green).

B. Test Accuracy

The results show that QMSVM can reach a comparable or higher classification accuracy with respect to its classical counterpart, i.e., CS SVM. This is a promising result, given the limitations discussed in Sect. V-A, in particular the small number of training examples M that QMSVM can handle in the optimization step. The reason is that the solution combination using N examples is able to improve the quality of the final solution on average by increasing N, as seen in the accuracy plots. However, the prediction accuracy of OVO and OVA is slightly higher on average than both CS and QMSVM for higher N. An even worse performance of QMSVM can be clearly seen on the more complex Potsdam dataset. The random selection method consistently outperforms k-means selection on Toulouse, while performing slightly better on Potsdam. This shows that k-means is inconsistent in practice and leaves an open question on the path to follow for an optimal example selection method. A high variance in accuracy with respect to the chosen training set should also be mentioned, which makes QMSVM more unstable than the compared standard SVM methods.

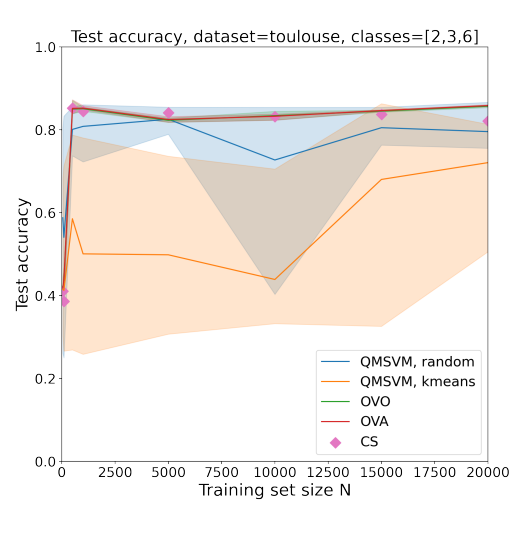
C. Time Complexity

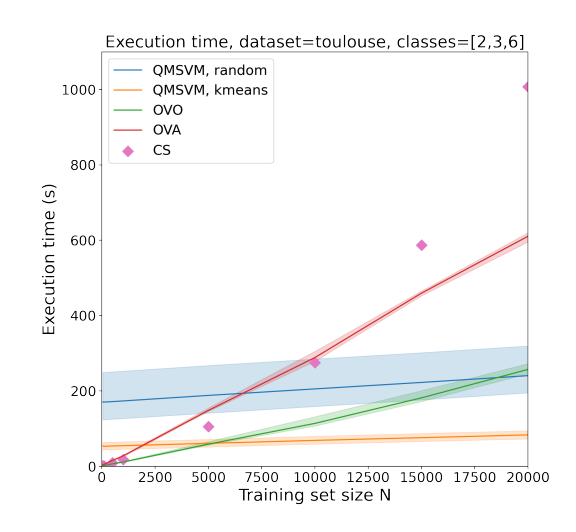
The most remarkable result is that the execution time of QMSVM for a high number of training examples N is lower than the execution time of the classical methods considered in the comparison. The different steps included in the measurement of the execution time are shown in detail in Fig. 9-10. It can be seen that the most demanding step in the QMSVM is the annealing step. The main reason is the high time complexity of the minor embedding algorithm [47] required

to run the QUBO problem on the quantum annealer. The interesting results are the linear time increase for the solution combination and the constant time for inference with respect to N. A theoretical explanation supporting the experimental results is summarized in the following.

In the solution combination step, the single solutions obtained by the annealer define S decision functions as in Eq. 16. The decision functions are evaluated on N examples and require the computation of the kernel values $K(x,x_m)$ with the M examples of the training subset. The evaluation is repeated for C classes and the class with highest value is chosen. For evaluating all the S classifiers, O(SCMN)operations are needed, leading to a linear time complexity with respect to the training set size. Similarly, the classifier used in the inference computes the kernel distances between the I test examples and the M training subset examples and it requires O(CMI) operations, i.e., it is independent from N. It is worth mentioning that the speedup of QMSVM is not strictly a quantum speedup. Instead, it is an algorithmic speedup related to the post-processing of the annealing solutions. The outcomes for OVO and OVA are also coherent with theory: the training complexity of the Scikit-learn SVM implementation is $O(N^3)$, whereas the inference time is linearly dependent on N [56].

These results clearly show that QMSVM is a much more scalable algorithm with respect to the considered training examples N compared to standard multiclass SVM methods. Given that the annealing step, which is a fixed step unrelated to N, has the largest impact in terms of time, the overall execution time can be regarded as near constant.

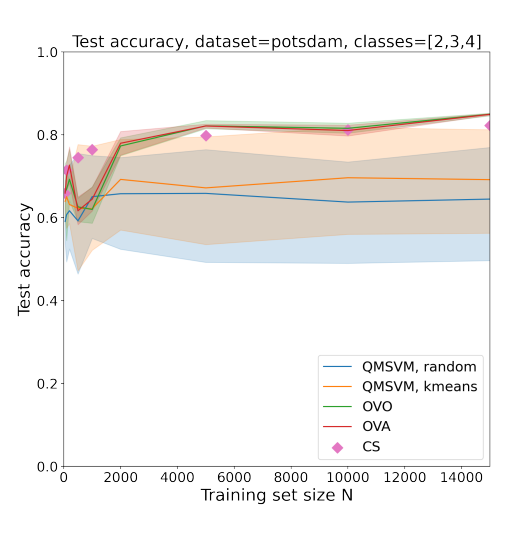


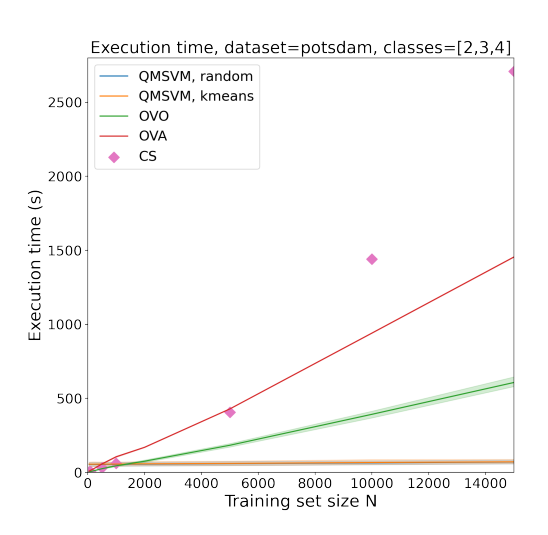


(a) Test accuracy vs. training set size N

(b) Execution time vs. training set size N

Fig. 7. Toulouse - test accuracy and execution time for Quantum Multiclass SVM (QMSVM), one-versus-one (OVO), one-versus-all (OVA) and Crammer-Singer SVM (CS) with respect to training set size N.





(a) Test accuracy vs. training set size N

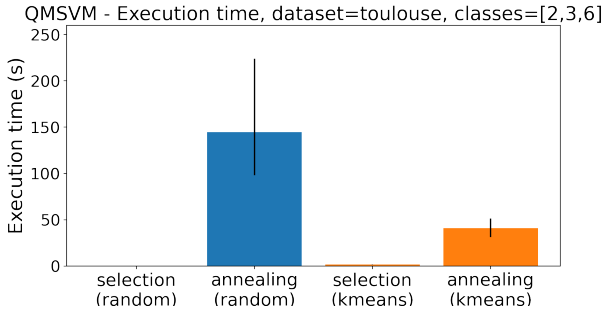
(b) Execution time vs. training set size N

Fig. 8. Potsdam - test accuracy and execution time for Quantum Multiclass SVM (QMSVM), one-versus-one (OVO), one-versus-all (OVA) and Crammer-Singer SVM (CS) with respect to training set size N.

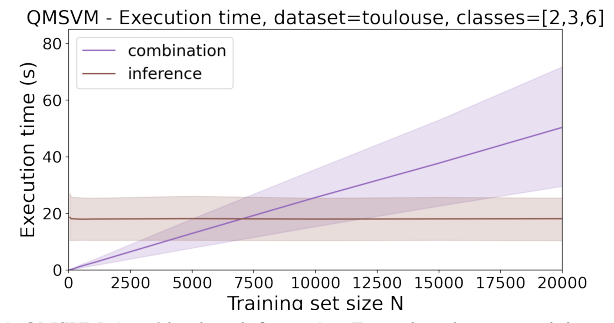
VI. CONCLUSIONS

QMSVM serves as a preliminary framework for applying QA to a single-step multiclass SVM algorithm, successfully leveraging the D-Wave Advantage quantum annealer in the training step. Although the results show that the prediction accuracy is not always higher than standard multiclass SVM algorithms trained on the same training set, especially using the more complex Potsdam dataset (compared to OVO: 0.8663 vs 0.8598 on Toulouse, 0.8123 vs 0.8521 on Potsdam), the improved scalability allows the usage of large-scale datasets, due to the lower total execution time (compared to OVO:

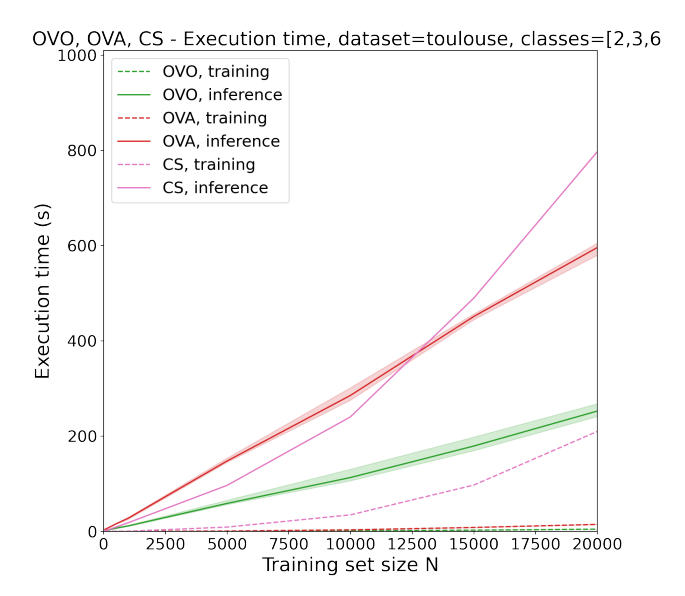
85.72s vs 248.02s on Toulouse, 58.89s vs 580.17s on Potsdam). Further research has to be conducted, in light of the promising achieved results. Time and accuracy analysis can be performed on different datasets, better assessing the impact of N and the model parameters on the prediction accuracy. A deeper analysis of different selection methods based on dataset representativeness, on top of the k-means method, can improve the quality of the solutions obtained by the QA. An improvement in performance for QMSVM is expected with the future development of QA, as a higher memory and qubit connectivity allows the usage of a larger training subset and enhances the quality of the obtained solutions.



(a) QMSVM (selection, annealing) - Execution time vs. training set size N



(b) QMSVM (combination, inference) - Execution time vs. training set size \ensuremath{N}

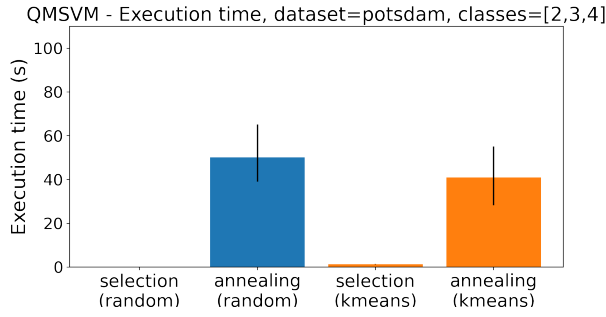


(c) OVO, OVA, CS - Execution time vs. training set size \boldsymbol{N}

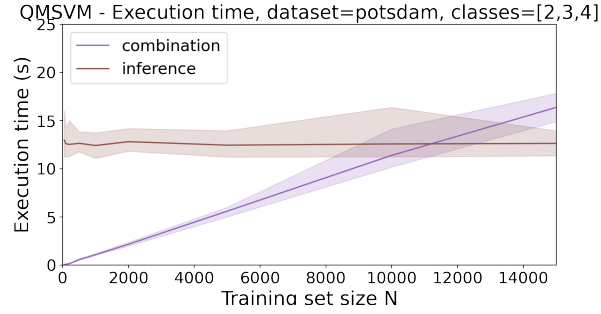
Fig. 9. Toulouse - execution time of each performed step, for Quantum Multiclass SVM (QMSVM), one-versus-one (OVO), one-versus-all (OVA) and Crammer-Singer SVM (CS), with respect to training set size N.

ACKNOWLEDGMENT

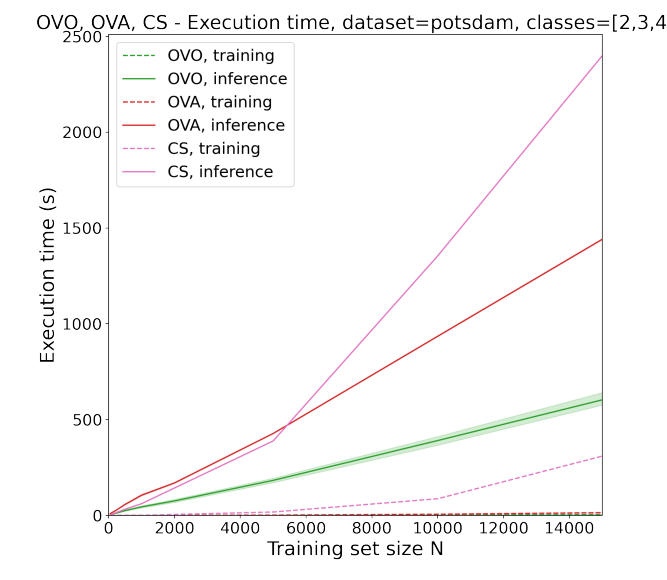
The authors gratefully acknowledge support from the project JUNIQ that has received funding from the German Federal Ministry of Education and Research (BMBF) and the Ministry of Culture and Science of the State of North Rhine-Westphalia. This work is part of the Quantum Computing for Earth Observation (QC4EO) initiative from the ESA Φ -lab and the Center of Excellence (CoE) Research on AI- and Simulation-Based Engineering at Exascale (RAISE) receiving funding



(a) QMSVM (selection, annealing) - Execution time vs. training set size N



(b) QMSVM (combination, inference) - Execution time vs. training set size N



(c) OVO, OVA, CS - Execution time vs. training set size N

Fig. 10. Potsdam - execution time of each performed step, for Quantum Multiclass SVM (QMSVM), one-versus-one (OVO), one-versus-all (OVA) and Crammer-Singer SVM (CS), with respect to training set size N.

from EU's Horizon 2020 Research and Innovation Framework Programme H2020-INFRAEDI-2019-1 under grant agreement no. 951733. This work is co-financed by the EUROCC2 project funded by the European High-Performance Computing Joint Undertaking (JU) and EU/EEA states under grant agreement No 101101903.

REFERENCES

[1] M. Chi, A. Plaza, J. A. Benediktsson, Z. Sun, J. Shen, and Y. Zhu, "Big Data for Remote Sensing: Challenges and Opportunities," *Proceedings*

- of the IEEE, vol. 104, pp. 2207-2219, Nov 2016.
- [2] M. A. Nielsen and I. L. Chuang, Quantum Computation and Quantum Information: 10th Anniversary Edition. Cambridge University Press, Dec. 2010.
- [3] R. Jozsa and N. Linden, "On the Role of Entanglement in Quantum-Computational Speed-Up," Proceedings of the Royal Society of London. Series A: Mathematical, Physical and Engineering Sciences, vol. 459, pp. 2011–2032, Aug. 2003.
- [4] T. F. Rønnow, Z. Wang, J. Job, S. Boixo, S. V. Isakov, D. Wecker, J. M. Martinis, D. A. Lidar, and M. Troyer, "Defining and Detecting Quantum Speedup," *Science*, vol. 345, no. 6195, pp. 420–424, 2014. [Online]. Available: https://www.science.org/doi/abs/10.1126/science.1252319
- [5] D. Aharonov, A. Kitaev, and N. Nisan, "Quantum Circuits with Mixed States," in *Proceedings of the thirtieth annual ACM symposium on Theory of computing*, 1998, pp. 20–30.
- [6] C. C. McGeoch, Adiabatic Quantum Computation and Quantum Annealing: Theory and Practice. Morgan & Claypool Publishers, 2014.
- [7] T. Albash and D. A. Lidar, "Adiabatic Quantum Computation," Rev. Mod. Phys., vol. 90, p. 015002, Jan 2018.
- [8] M. Born and V. Fock, "Beweis des Adiabatensatzes," Zeitschrift für Physik 1928 51:3, vol. 51, pp. 165–180, Mar. 1928.
- [9] D. Aharonov, W. van Dam, J. Kempe, Z. Landau, S. Lloyd, and O. Regev, "Adiabatic Quantum Computation is Equivalent to Standard Quantum Computation," SIAM Review, vol. 50, no. 4, p. 755–787, 2008.
- [10] T. Kadowaki and H. Nishimori, "Quantum Annealing in the Transverse Ising Model," *Physical Review E*, vol. 58, no. 5, pp. 5355–5363, 1998.
- [11] A. Finnila, M. Gomez, C. Sebenik, C. Stenson, and J. Doll, "Quantum Annealing: A New Method for Minimizing Multidimensional Functions," *Chemical Physics Letters*, vol. 219, no. 5, pp. 343–348, 1994.
- [12] J. Biamonte, P. Wittek, N. Pancotti, P. Rebentrost, N. Wiebe, and S. Lloyd, "Quantum Machine Learning," *Nature*, vol. 549, no. 7671, pp. 195–202, 2017.
- [13] V. Dunjko and H. J. Briegel, "Machine Learning and Artificial Intelligence in the Quantum Domain: a Review of Recent Progress," *Reports on Progress in Physics*, vol. 81, no. 7, p. 074001, jun 2018.
- [14] R. Y. Li, R. D. Felice, R. Rohs, and D. A. Lidar, "Quantum Annealing versus Classical Machine Learning Applied to a Simplified Computational Biology Problem," npj Quantum Information 2018 4:1, vol. 4, pp. 1–10. Feb. 2018.
- [15] P. Gawron and S. Lewiński, "Multi-Spectral Image Classification with Quantum Neural Network," in *IGARSS* 2020 - 2020 IEEE International Geoscience and Remote Sensing Symposium, 2020, pp. 3513–3516.
- [16] A. Sebastianelli, D. A. Zaidenberg, D. Spiller, B. L. Saux, and S. L. Ullo, "On Circuit-Based Hybrid Quantum Neural Networks for Remote Sensing Imagery Classification," *IEEE Journal of Selected Topics in Applied Earth Observations and Remote Sensing*, vol. 15, pp. 565–580, 2022.
- [17] F. Fan, Y. Shi, and X. X. Zhu, "Urban Land Cover Classification from Sentinel-2 Images with Quantum-Classical Network," in 2023 Joint Urban Remote Sensing Event (JURSE), 2023, pp. 1–4.
- [18] M. van Waveren, M. Savinaud, G. Pasero, V. Defonte, P.-M. Brunet, O. Faucoz, P. Gawron, B. Gardas, Z. Puchala, and L. Pawela, "Comparison of Quantum Neural Network Algorithms For Earth Observation Data Classification," in *IGARSS* 2023 - 2023 IEEE International Geoscience and Remote Sensing Symposium, 2023, pp. 780–783.
- [19] S. Otgonbaatar and M. Datcu, "A Quantum Annealer for Subset Feature Selection and the Classification of Hyperspectral Images," *IEEE Journal* of Selected Topics in Applied Earth Observations and Remote Sensing, vol. 14, pp. 7057–7065, 2021.
- [20] —, "Classification of Remote Sensing Images with Parameterized Quantum Gates," *IEEE Geoscience and Remote Sensing Letters*, vol. 19, 2022.
- [21] S. Otgonbaatar, G. Schwarz, M. Datcu, and D. Kranzlmüller, "Quantum Transfer Learning for Real-World, Small, and High-Dimensional Datasets," 2022, arXiv:2209.07799.
- [22] R. U. Shaik and S. Periasamy, "Accuracy and Processing Speed Tradeoffs in Classical and Quantum SVM Classifier Exploiting PRISMA Hyperspectral Imagery," *International Journal of Remote Sensing*, vol. 43, no. 15-16, pp. 6176–6194, 2022.
- [23] M. K. Gupta, M. Romaszewski, and P. Gawron, "Potential of Quantum Machine Learning for Processing Multispectral Earth Observation Data," *TechRxiv*, 2023.
- [24] A. Miroszewski, J. Mielczarek, G. Czelusta, F. Szczepanek, B. Grabowski, B. Le Saux, and J. Nalepa, "Detecting Clouds in Multispectral Satellite Images Using Quantum-kernel Support Vector Machines," *IEEE Journal of Selected Topics in Applied Earth Observations and Remote Sensing*, 2023.

- [25] A. G. Pai, K. M. Buddhiraju, and S. S. Durbha, "Multiclass Classification of Hyperspectral Remote Sensed Data using QSVC," in *Remote Sensing* for Agriculture, Ecosystems, and Hydrology XXIV, C. M. U. Neale and A. Maltese, Eds., vol. 12262, International Society for Optics and Photonics. SPIE, 2022, p. 122620P.
- [26] S. Huber, K. Glatting, G. Krieger, and A. Moreira, "Quantum Annealing for SAR System Design and Processing," in EUSAR 2022; 14th European Conference on Synthetic Aperture Radar, 2022.
- [27] S. Otgonbaatar and M. Datcu, "Quantum Annealer for Network Flow Minimization in InSAR Images," in EUSAR 2021; 13th European Conference on Synthetic Aperture Radar, 2021, pp. 1–4.
- [28] ——, "Natural Embedding of the Stokes Parameters of Polarimetric Synthetic Aperture Radar Images in a Gate-Based Quantum Computer," *IEEE Transactions on Geoscience and Remote Sensing*, 2021.
- [29] G. Cavallaro, D. Willsch, M. Willsch, K. Michielsen, and M. Riedel, "Approaching Remote Sensing Image Classification with Ensembles of Support Vector Machines on the D-Wave Quantum Annealer," in Proceedings of the IEEE IGARSS, 2020, pp. 1973–1976.
- [30] A. Delilbasic, G. Cavallaro, M. Willsch, F. Melgani, M. Riedel, and K. Michielsen, "Quantum Support Vector Machine Algorithms for Remote Sensing Data Classification," in *Proceedings of the IEEE IGARSS*. Institute of Electrical and Electronics Engineers (IEEE), Dec. 2021.
- [31] Y. Ma and G. Guo, Support Vector Machines Applications. Springer, 2014, vol. 649.
- [32] F. Melgani and L. Bruzzone, "Classification of Hyperspectral Remote Sensing Images with Support Vector Machines," *IEEE Transactions on Geoscience and Remote Sensing*, vol. 42, no. 8, pp. 1778–1790, 2004.
- [33] C.-W. Hsu and C.-J. Lin, "A Comparison of Methods for Multiclass Support Vector Machines," *IEEE Transactions on Neural Networks*, vol. 13, no. 2, pp. 415–425, 2002.
- [34] A. K. Bishwas, A. Mani, and V. Palade, "An All-Pair Quantum SVM Approach for Big Data Multiclass Classification," *Quantum Information Processing*, vol. 17, pp. 1–16, Oct 2018.
- [35] B. A. Dema, J. Arai, and K. Horikawa, "Support Vector Machine for Multiclass Classification using Quantum Annealers," in *Proceedings of the DEIM Forum*, 2020.
- [36] X.-J. Yuan, Z.-Q. Chen, Y.-D. Liu, Z. Xie, X.-M. Jin, Y.-Z. Liu, X. Wen, and H. Tang, "Quantum Support Vector Machines for Aerodynamic Classification," 2022, arXiv:2208.07138.
- [37] P. Rebentrost, M. Mohseni, and S. Lloyd, "Quantum Support Vector Machine for Big Data Classification," *Physical Review Letters*, vol. 113, no. 13, 2014.
- [38] R. Zhang, J. Wang, N. Jiang, H. Li, and Z. Wang, "Quantum Support Vector Machine Based on Regularized Newton Method," *Neural Networks*, vol. 151, pp. 376–384, 2022.
- [39] V. Havlíček, A. D. Córcoles, K. Temme, A. W. Harrow, A. Kandala, J. M. Chow, and J. M. Gambetta, "Supervised Learning with Quantum-Enhanced Feature Spaces," *Nature*, vol. 567, no. 7747, pp. 209–212, 2019.
- [40] D. Willsch, M. Willsch, H. D. Raedt, and K. Michielsen, "Support Vector Machines on the D-Wave Quantum Annealer," *Computer Physics Communications*, vol. 248, Jun 2019.
- [41] K. Crammer and Y. Singer, "On the Algorithmic Implementation of Multiclass Kernel-Based Vector Machines," *J. Mach. Learn. Res.*, vol. 2, p. 265–292, Mar. 2002.
- [42] J. Weston and C. Watkins, "Multi-class Support Vector Machines," Proceedings of the Seventh European Symposium on Artificial Neural Networks, 1998.
- [43] Z. Wang and X. Xue, "Multi-class Support Vector Machine," Support Vector Machines Applications, pp. 23–48, 2014.
- [44] D-Wave Systems, https://www.dwavesys.com/, accessed: 08/01/2023.
- [45] C. McGeoch and P. Farré, "The Advantage System: Performance Update," D-Wave Systems, Tech. Rep., 2021.
- [46] P. J. M. van Laarhoven and E. H. L. Aarts, Simulated Annealing. Dordrecht: Springer Netherlands, 1987, pp. 7–15.
- [47] J. Cai, W. G. Macready, and A. Roy, "A Practical Heuristic for Finding Graph Minors," 2014, arXiv:1406.2741.
- [48] R. Roscher, M. Volpi, C. Mallet, L. Drees, and J. D. Wegner, "SemCity Toulouse: a Benchmark for Building Instance Segmentation in Satellite Images," ISPRS Annals of Photogrammetry, Remote Sensing and Spatial Information Sciences, vol. V-5-2020, pp. 109–116, 2020.
- [49] ISPRS, "2D Semantic Labeling Contest Potsdam," https://www.isprs.org/education/benchmarks/UrbanSemLab/2d-sem-label-potsdam.aspx, accessed: 08/01/2023.
- [50] Forschungszentrum Jülich, https://www.fz-juelich.de/en/ias/jsc/systems/ quantum-computing/juniq-facility/juniq/d-wave-advantagetm-systemjupsi, accessed: 08/01/2023.

- [51] J. A. Hartigan and M. A. Wong, "Algorithm AS 136: A K-Means Clustering Algorithm," *Journal of the Royal Statistical Society. Series* C (Applied Statistics), vol. 28, no. 1, pp. 100–108, 1979.
- [52] D.-S. Huang, K. Li, G. W. Irwin, S.-J. Yen, and Y.-S. Lee, "Under-Sampling Approaches for Improving Prediction of the Minority Class in an Imbalanced Dataset," *Intelligent Control and Automation*, vol. 344, pp. 731–740, 10 2006.
- [53] F. Pedregosa, G. Varoquaux, A. Gramfort, V. Michel, B. Thirion, O. Grisel, M. Blondel, P. Prettenhofer, R. Weiss, V. Dubourg, J. Vanderplas, A. Passos, D. Cournapeau, M. Brucher, M. Perrot, and E. Duchesnay, "Scikit-learn: Machine Learning in Python," *Journal of Machine Learning Research*, vol. 12, pp. 2825–2830, 2011.
- [54] T. Joachims, "SVM-Multiclass: Multi-Class Support Vector Machine," https://www.cs.cornell.edu/people/tj/svm_light/svm_multiclass.html, accessed: 08/01/2023.
- [55] D. Willsch, M. Willsch, C. D. G. Calaza, F. Jin, H. D. Raedt, M. Svensson, and K. Michielsen, "Benchmarking Advantage and D-Wave 2000Q quantum annealers with exact cover problems," *Quantum Information Processing*, vol. 21, pp. 1–22, 4 2022.
- [56] A. Ns and R. Wardoyo, "Time Complexity Analysis of Support Vector Machines (SVM) in LibSVM," *International Journal of Computer Applications*, vol. 128, pp. 975–8887, Oct 2015.



Morris Riedel (Member, IEEE) received his PhD from the Karlsruhe Institute of Technology (KIT) and worked in data-intensive parallel and distributed systems since 2004. He is currently a Full Professor of High-Performance Computing with an emphasis on Parallel and Scalable Machine Learning at the School of Natural Sciences and Engineering of the University of Iceland. Since 2004, Prof. Dr. - Ing. Morris Riedel held various positions at the Juelich Supercomputing Centre of Forschungszentrum Juelich in Germany. In addition, he is the Head

of the joint High Productivity Data Processing research group between the Juelich Supercomputing Centre and the University of Iceland. Since 2020, he is also the EuroHPC Joint Undertaking governing board member for Iceland. His research interests include high-performance computing, remote sensing applications, medicine and health applications, pattern recognition, image processing, and data sciences, and he has authored extensively in those fields. Prof. Dr. – Ing. Morris Riedel online YouTube and university lectures include High-Performance Computing – Advanced Scientific Computing, Cloud Computing and Big Data – Parallel and Scalable Machine and Deep Learning, as well as Statistical Data Mining. In addition, he has performed numerous hands-on training events in parallel and scalable machine and deep learning techniques on cutting-edge HPC systems.



Amer Delilbasic (Student Member, IEEE) received the B.Sc. and M.Sc. degrees in information and communication engineering from the University of Trento in 2019 and 2021, respectively. He is member of the "AI and ML for Remote Sensing" Simulation and Data Lab at the Jülich Supercomputing Centre, Forschungszentrum Jülich, Germany. He is currently pursuing the Ph.D. degree in computational engineering at the University of Iceland. He is an external researcher at Φ-lab, European Space Agency, Frascati, Italy. His research interest is mainly in

machine learning methods for remote sensing applications, with a particular focus on Quantum Computing (QC) and High Performance Computing (HPC).



Kristel Michielsen received her PhD from the University of Groningen, the Netherlands, for work on the simulation of strongly correlated electron systems in 1993. Since 2009 she is group leader of the research group Quantum Information Processing at the Jülich Supercomputing Centre, Forschungszentrum Jülich (Germany) and is also Professor of Quantum Information Processing at RWTH Aachen University (Germany). Her current research interests include quantum computation, quantum annealing, quantum statistical physics, event-based simulation

methods of quantum phenomena, logical inference approach to quantum mechanics and computational electrodynamics.



Bertrand Le Saux (Senior Member, IEEE) received the Ms.Eng. and M.Sc. degrees from INP, Grenoble, France, in 1999, the Ph.D. degree from the University of Versailles/Inria, Versailles, France, in 2003, and the Dr. Habil. degree from the University of Paris-Saclay, Saclay, France, in 2019. He is a Senior Scientist with the European Space Agency/European Space Research Institute Φ-lab in Frascati, Italy. His research interest aims at visual understanding of the environment by data-driven techniques including Artificial Intelligence and (Quantum) Machine

Learning. He is interested in tackling practical problems that arise in Earth observation, to bring solutions to current environment and population challenges. Dr. Le Saux is an Associate Editor of the Geoscience and Remote Sensing Letters. He was Co-Chair (2015–2017) and chair (2017–2019) for the IEEE GRSS Technical Committee on Image Analysis and Data Fusion.



Gabriele Cavallaro (Senior Member, IEEE) received his B.Sc. and M.Sc. degrees in Telecommunications Engineering from the University of Trento, Italy, in 2011 and 2013, respectively, and a Ph.D. degree in Electrical and Computer Engineering from the University of Iceland, Iceland, in 2016. From 2016 to 2021 he has been the deputy head of the "High Productivity Data Processing" (HPDP) research group at the Jülich Supercomputing Centre (JSC), Forschungszentrum Jülich, Germany. Since 2022, he is the Head of the "AI and ML for Remote

Sensing" Simulation and Data Lab at the JSC and an Adjunct Associate Professor with the School of Natural Sciences and Engineering, University of Iceland, Iceland. From 2020 to 2023, he held the position of Chair for the High-Performance and Disruptive Computing in Remote Sensing (HDCRS) Working Group under the IEEE GRSS Earth Science Informatics Technical Committee (ESI TC). In 2023, he took on the role of Co-chair for the ESI TC. Concurrently, he serves as Visiting Professor at the Φ -lab within the European Space Agency (ESA), where he contributes to the Quantum Computing for Earth Observation (QC4EO) initiative. Additionally, he has been serving as an Associate Editor for the IEEE Transactions on Image Processing (TIP) since October 2022. He was the recipient of the IEEE GRSS Third Prize in the Student Paper Competition of the IEEE International Geoscience and Remote Sensing Symposium (IGARSS) 2015 (Milan - Italy). His research interests include remote sensing data processing with parallel machine learning algorithms that scale on distributed computing systems and innovative computing technologies.